

Article

Free Vibration Analyses of Stiffened Functionally Graded Graphene-Reinforced Composite Multilayer Cylindrical Panel

Yuhua Zhou ¹, Yanhu Zhang ¹, Brighton Nyasha Chirukam ², Jianwei Li ^{1,*}, Congshan Lu ³, Masoud Babaei ^{4,*} and Kamran Asemi ⁵ 

¹ Institute of Advanced Manufacturing and Modern Equipment Technology, Jiangsu University, Zhenjiang 212000, China; zhou839@yahoo.com (Y.Z.); yanhuzhang08121@gmail.com (Y.Z.)

² School of Mechanical Engineering, Xi'an Technological University, Xi'an 710021, China; brightonnchirukam05686@gmail.com

³ School of Mechanical Engineering, Jiangsu University, Zhenjiang 212000, China; congshanlu01@gmail.com

⁴ Department of Mechanical Engineering, University of Eyvanekey, Eyvanekey 99888-35918, Iran

⁵ Department of Mechanical Engineering, Islamic Azad University, North Tehran Branch, Tehran 1477893855, Iran; k.asemi@iau-tnb.ac.ir

* Correspondence: ujs_zhyh@126.com (J.L.); masoudbabaei@eyc.ac.ir (M.B.)

Abstract: In this paper, the free vibration response of a stiffened functionally graded graphene nanoplatelet (GPL)-reinforced composite multilayer cylindrical shell panel is studied for the first time. The shell is stiffened by both stringers and rings. Additionally, the effect of reinforcing the shell panel, ring and stinger with GPLs is independently studied. Halpin–Tsai relations are employed to evaluate the mechanical properties of the shell panel, rings and stringers. The first-order shear deformation shell theory, accompanied by the Lekhnitsky smeared stiffener model, using the numerical finite element method and Hamilton principle, is employed to develop the governing motion equations of the shell panel. Four different types of GPL patterns, including FG-A, FG-X, FG-O and UD, are assumed across the thickness of the shell panel, rings and stringers. The effects of different factors, including various weight fractions and patterns of GPLs nanofillers, the geometry of the shell panel and stiffeners and two displacement boundary conditions, on the natural frequencies of the shell panel, have been studied.

Keywords: free vibration; stiffened; functionally graded; graphene-reinforced composite multilayer cylindrical panel; FSDT; FEM

MSC: 37M05



Citation: Zhou, Y.; Zhang, Y.; Nyasha Chirukam, B.; Li, J.; Lu, C.; Babaei, M.; Asemi, K. Free Vibration Analyses of Stiffened Functionally Graded Graphene-Reinforced Composite Multilayer Cylindrical Panel. *Mathematics* **2023**, *11*, 3662. <https://doi.org/10.3390/math11173662>

Academic Editors: Joaquim Infante Barbosa and José Alberto Rodrigues

Received: 1 August 2023

Revised: 18 August 2023

Accepted: 22 August 2023

Published: 24 August 2023



Copyright: © 2023 by the authors. Licensee MDPI, Basel, Switzerland. This article is an open access article distributed under the terms and conditions of the Creative Commons Attribution (CC BY) license (<https://creativecommons.org/licenses/by/4.0/>).

1. Introduction

Nowadays, reinforcement plays an important role in different industries, such as aerospace, marine and automotive industries. These reinforcements can be divided into two major groups. In the first group, the structure is stiffened by another external shape, such as a ring or stringer. The external stiffener can be fabricated with the same or different material as the original structure. These stiffeners can be connected to the original structure with glue, welding, screws or rivets. Due to the fact that these connections may cause a stress concentration, the original structure and stiffeners can be manufactured integrally. In the second group, the structure is reinforced with nanoparticles. These nanoparticles are added to the metallic or polymeric matrix during the process of fabrication, and metallic or polymeric nanocomposite structures are manufactured. These reinforcements can be added to various shapes, including plate, beam and shell-type structures and increase the dynamic and static efficiency of the structure. Among these structures, shell-type structures are widely applied as a part of sophisticated shapes, such as aircraft, rockets, submarines, etc. Due to these structures being continuously subjected to dynamic loads, it

is essential to study the vibration response and natural frequencies of shell-type-reinforced structures. There are a lot of investigations related to the natural frequency responses of stiffened structures. First, the articles are reviewed that are related to the vibration behavior of the first group. For instance, natural frequencies of ring-and-stringer-stiffened conical shells with simply supported boundary conditions are presented numerically and experimentally by Crenwelge and Muster [1]. Nayak, Satpathy and Tripathy [2] presented free vibrations of stiffened plates using the numerical finite element method (FEM). The effect of several parameters, such as the number and orientation of stiffeners, aspect ratio, boundary conditions and stiffener depth to plate thickness ratio on the free vibration of stiffened plates are investigated. Based on laminated composite shell theories and utilizing FEM, Nayak and Bandyopadhyay [3] performed a comprehensive investigation of the free vibration responses of laminated composite stiffened shallow shells. Sinha et al. [4] employed experimental and numerical approaches to present the natural frequencies of laminated composite stiffened plates by changing the numbers, types and orientation of stiffeners. Nayak and Bandyopadhyay [5] developed an FE formulation for the natural frequency characteristics of stiffened conoidal shells. The effects of various stiffened geometries on the free vibration response of conoidal shells were examined. The free vibration response of shells of revolution stiffened by stringers employing a finite strip method was reported by Naghsh, Saadatpour and Azhari [6]. They understood that reinforcing the shells with stringers could increase or decrease the natural frequency. Quoc, Van Tham and Tu [7] studied the free vibration behavior of a stiffened functionally graded (FG) porous cylindrical shell under different boundary conditions on the basis of first-order shear deformation theory (FSDT), Lekhnitsky's smeared stiffener assumptions and the Galerkin method. Samanta and Mukhopadhyay [8] surveyed the natural frequencies of stiffened shells by applying FSDT and the FE technique. Mustafa and Ali [9] applied an energy method for the natural frequencies of stiffened circular cylindrical shells based on FSDT. Al-Najafi and Warburton [10] presented the natural frequency characteristics of ring-stiffened cylindrical shells by applying Flügge's shell theory and using the Rayleigh–Ritz approach. Zarei, Rahimi and Hemmatnezhad [11] performed a comprehensive investigation, including numerical, experimental and analytical approaches, to evaluate natural frequencies of grid-stiffened truncated composite conical shells using FSDT. Their analytical procedure was conducted in accordance with the Ritz method. Additionally, Zarei, Rahimi and Hemmatnezhad [12] used the same methodology and solution to investigate the free vibration response of stiffened composite joined conical–cylindrical shells. Aris and Ahmadi [13] performed an investigation on the natural frequency results of stiffened rotating FGM conical shells under thermal conditions in accordance with higher-order shear deformation theory (HSDT) and applying the Galerkin method. Based on Donnell's thin shell theory and employing the Galerkin procedure, the free vibration behavior of grid-stiffened composite truncated spherical shells was reported by Ansari, Hemmatnezhad and Taherkhani [14]. Tu Tran et al. [15] employed FSDT, together with the Galerkin method and Lekhnitsky's smeared stiffener technique, to analyze natural frequencies of stiffened FG circular cylindrical shells supported by a Pasternak elastic foundation for various boundary conditions subjected to a thermal environment. The free vibration analysis of laminated stiffened cylindrical panels based on FSDT and utilizing FEM was surveyed by Tuan, Quoc and Tu, [16]. Nguyen and Hoang [17] analytically presented the free vibration response of a stiffened FG cylindrical shell supported on an elastic foundation based on FSDT, the Galerkin method and the Lekhnitsky smeared stiffener technique. Qin Li et al. [18] employed FSDT and an analytical solution based on Rayleigh–Ritz to study the free vibration of a stiffened cylindrical shell under general boundary conditions. Bich, Van Dung and Nam [19] investigated the vibration response of eccentrically stiffened FG cylindrical panels based on classical shell theory by employing the analytical method. The natural frequency response of stiffened cylindrical shells in accordance with higher-order theory determined by applying the Carrera unified formulation (CUF) was examined by Carrera, Zappino and Filippi [20]. Lugovoi and Prokopenko [21] studied the impact of an elastic foundation

and reinforcement on the vibration response of shallow shells with a rectangular planform. Shahani and Kiarasi [22] studied the influence of a ring and stringer on the stability of thin cylindrical shells based on FSDT numerically and experimentally.

This literature review denotes that in the most of research, the connection between the original structure and reinforcements is considered ideal without screws, rivets and welding. Therefore, in most of them, Lekhnitsky's smeared stiffener technique is applied for analysis. Now, the articles are reviewed which are related to the second group of reinforcements or to reinforcing with nanoparticles. As lots of investigations have been developed for the dynamic and static analyses of the structures which are reinforced with various nanoparticles, those studies are mentioned here that are related to the vibration behavior of plate and shell-type structures which are reinforced by Graphene platelets (GPLs). In detail, the vibration responses of polymeric composite shells reinforced by GPLs integrated with piezoelectric patches including electroelastic nonlinearities were presented by Rao, Schmidt and Schröder [23]. Van Do and Lee [24] employed the Bézier extraction-based isogeometric method to predict the natural frequencies of FG-GPLs multilayered composite cylindrical shell panels by applying FSDT. Amirabadi, Farhatnia, Eftekhari and Hosseini-Ara [25] used third-order shear deformation theory (TSDT) and the generalized differential quadrature method (GDQM) to obtain the free vibration responses of FG-GPL-reinforced conical shells under a rotational velocity and various displacement boundary conditions. Jamalabadi et al. [26] calculated the fundamental natural frequencies of FG-GPL-reinforced composite conical panels supported by an elastic foundation using FSDT and 2D-GDQ methods. Salehi, Gholami and Ansari [27] presented the nonlinear free vibration response of FG porous cylindrical shells reinforced by GPLs considering initial imperfections utilizing HSDT. Yang et al. [28] employed FSDT, the Galerkin approach and harmonic balance method to predict the nonlinear free vibration results of FG-GPL-reinforced composite conical shells. Van Do and Lee [29] developed HSDT to investigate static response and the natural frequencies of multilayer spherical and cylindrical panels reinforced by GPLs in accordance with the isogeometric procedure. Employing FSDT and Ritz's method, the free vibration of GPL-reinforced composite doubly curved shells was presented by Esmaili and Kiani [30]. Baghbadorani and Kiani [31] used the Donnell kinematic relations, FSDT and Navier solutions for the free vibration response of FG cylindrical shells reinforced with GPLs. Dong et al. [32] studied the influences of axial load and rotational velocity on the nonlinear free vibration response of graded-graphene-reinforced cylindrical shells based on the nonlinear Donnell shell theory and by employing the Galerkin approach. Based on a similar methodology and solution, the natural frequency responses of FG-GPL-reinforced porous nanocomposite cylindrical shells with rotational velocity were presented by Dong et al. [33]. Song et al. [34] employed the second-order shear deformation theory in curvilinear coordinate and analytical solution based on harmonic response to investigate wave dispersion responses of FG-GPL curved viscoelastic panels. Sobhani et al. [35] employed FSDT and GDQ methods to evaluate the vibration behavior of graphene oxide powder composites joined paraboloidal–cylindrical shells with different boundary conditions. The effect of initial imperfection on the active control of FG-GPL cylindrical shells with piezoelectric layers due to the application of a proportional derivative smart controller was reported by Zare et al. [36].

Rezaei Pajand, Sobhani and Masoodi [37] investigated the vibrational response of joined conical–conical shells made of FGM based on FSDT and employing the GDQM. In another work, based on the same theory and methodology, Sobhani and Avcar [38] performed an investigation on the influence of various nanofiller materials (CNTs, GNPs, and GOPs) on the natural frequencies of nanocomposite cylindrical shells. Sobhani, Masoodi and Ahmad Pari [39] analyzed the free-damped vibration of GPL nanocomposite joined conical–conical–cylindrical-shell marine-like structures in accordance with FSDT and Donnell's simplifications. The governing equations of the structure were obtained by employing the Hamilton principle. Finally, GDQM was applied for solving the governing equations of the structure. Based on the first-order shear deformation hypothesis and

GDQM, wave frequency responses of the nanocomposite-linked hemispherical–conical-shell underwater-like bodies with the impacts of two types of graphene-based nanofillers were reported by Sobhani, Masoodi and Ahmad Pari [40]. Sobhani, Masoodi and Ahmad Pari [41] employed FDST as the theory and GDQM as a solution to evaluate the circumferential vibration analysis of nano-porous-sandwich assembled spherical–cylindrical–conical shells under elastic boundary conditions. Sobhani, Masoodi and Civalek [42] simulated the vibrational response of a jet engine cowl shell-like structure based on FSDT by employing GDQM as a numerical approach. Sobhani [43] used (FSDT) and the general shell hypothesis (GSH) to investigate the free vibration of combined paraboloidal–conical air vehicle segment shell-type structures. The governing equations of the structure were obtained by employing the Hamilton principle. Finally, GDQM was applied for solving the governing equations of combined paraboloidal–conical air vehicle segment shell-type structures. Song et al. [44] presented an analytical solution based on the perturbation technique to investigate buckling and postbuckling of biaxially compressed functionally graded multi-layer graphene nanoplatelet-reinforced polymer composite plates. Within the framework of the first-order shear deformation plate theory, Song et al. [45] presented an analytical solution based on the Navier method for the free and forced vibrations of functionally graded polymer composite plates reinforced with graphene nanoplatelets. Wang, Ye and Zu [46] studied the nonlinear vibration of metal foam cylindrical shells reinforced with graphene platelets based on the improved Donnell nonlinear shell theory by applying the Galerkin approach. Chai and Wang [47] presented an analytical solution for the traveling wave vibration of graphene platelet-reinforced porous joined conical–cylindrical shells in a spinning motion based on Donnell’s shell theory. Ye and Wang [48] employed the Galerkin procedure and Donnell’s nonlinear shell theory to analyze the nonlinear forced vibration of functionally graded graphene platelet-reinforced metal foam cylindrical shells: internal resonances. By using the Galerkin method, the nonlinear forced vibration of the simply supported functionally graded porous nanocomposite thin plates reinforced with graphene platelets based on the Kirchhoff assumptions was presented by Teng and Wang [49]. Wang et al. [50] presented an efficient method for the vibration and stability analysis of rectangular plates axially moving in fluid based on the Kirchhoff plate theory and utilizing the finite element method. Based on Donnell’s shell theory and using the Rayleigh–Ritz method, a general approach for the free vibration analysis of spinning joined conical–cylindrical shells with arbitrary boundary conditions was examined by Chai and Wang [51]. Safarpour, Rahimi and Alibeigloo [52] studied the free vibration and static responses of FG-GPL-truncated conical and cylindrical shells by applying 3D elasticity theory and using GDQM as a solution method. Babaei et al. [53] presented the natural frequency responses of a FG-GPL cylindrical shell panel based on the 3D theory of elasticity by applying FEM according to the Rayleigh–Ritz approach. Based on the same procedure and solution, Kiarasi et al. [54] investigated the free vibration of FG-GPL joined conical–cylindrical shells. Zhang, Wang and Li [55] used FEM, the 3D theory of elasticity and the Rayleigh–Ritz method to calculate the natural frequencies amounts of FG-GPL joined hemispherical–cylindrical–hemispherical shell vessels. Zu et al. [56] analyzed the vibration suppression performance of fiber-reinforced polymer spherical–cylindrical shells with GPL coatings under thermal conditions by applying the FSDT and Rayleigh–Ritz technique.

The above literature review shows that reinforcing the structures with nanoparticles and stiffening them using a ring and stringer have a great effect on the natural frequency response of the structures, but no investigation has been presented pertaining to the effect of both of them on the behavior of the structures yet. In this study, the free vibration of stiffened functionally graded graphene-reinforced composite multilayer cylindrical shell panels has been investigated for the first time. In this study, the shell panel, rings and stringers are reinforced with GPLs independently. Reinforcing the rings and stringers in addition to the shell panel is one of the novel points of the present study. Four various distributions of GPLs across the thickness of cylindrical panel, rings and stringers are considered. Lekhnitsky’s smeared stiffener technique is assumed for obtaining the governing equations

of the stiffened FG-GPL cylindrical shell panel. By employing the Hamilton principle in conjunction with FSDT, the governing motion equations of the shell are developed and solved via FEM. The effects of several factors such as the weight fractions of GPLs, various GPL patterns for the cylindrical panel, rings and stringers, different boundary conditions, and the effect of the geometry of the panel and stiffeners on the natural frequencies of stiffened FG-GPL cylindrical shell panel have been investigated. In detail, the maximum influences of the GPL pattern and the weight fraction of GPLs on the natural frequencies of the structure were approximately 60% and 118%, respectively. Additionally, the influence of strengthening the shell with GPLs was much greater than that of stiffening it with ring and stringers.

2. Deriving the Governing Equations

2.1. Definition of the Geometry and Material Properties of the Stiffened Cylindrical Shell Panel

Consider an FG-GPL multilayer cylindrical shell panel with stiffeners under compressive axial force (Figure 1). The radius, length, span angle and thickness of the structure are denoted by L , β and h , respectively. Additionally, (x, θ, z) is considered across the axial, hoop and radial axes, respectively. The shell panel is stiffened by both stringers (longitudinal stiffeners) and rings (circumferential stiffeners). Additionally, various GPL patterns are shown in Figure 1.

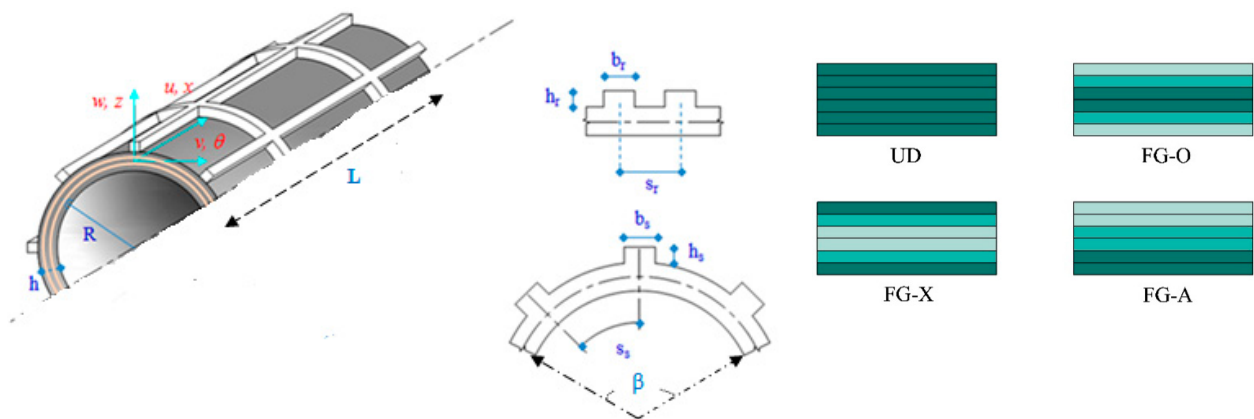


Figure 1. The geometry of the stiffened FG-GPL multilayer shell panel and the different distributions of the GPLs.

The multilayer GPL nanocomposite shell panel is assumed to have excellently bonded GPL-RC layers. In this research, it is considered that the shell panel is reinforced by GPLs. Each layer of the shell panel consists of a combination of GPLs as a nanofiller and a matrix made of an isotropic polymer. Due to the elimination of the stress concentration, rings and stringers are made of the same isotropic polymeric matrix used in the shell panel. GPLs are uniformly or non-uniformly distributed in the polymer matrix. Hence, the weight fraction of the nano-fillers (GPLs) varies in terms of being functionally graded across the radial direction of the shell panel. It is supposed that the shell panel is constructed of NL layers. Four different functions of the volume fraction of FG GPL-RCs are considered: FG-A, O, X, and a uniform pattern (UD). For UD, the GPL weight fraction is the same for each layer. Therefore, UD represents a homogeneous isotropic GPL-RC structure. In the FG patterns, the weight fraction of GPL has a linear variation across the thickness of the shell panel. For FG-X, the weight fraction of GPLs at the inner and outer layers is the maximum while this is different for the FG-O where the weight fraction for mid-layers is the maximum. Furthermore, for A-GPLRC, the weight fraction at the inner layers is the maximum and by distancing from it, the number of GPLs continuously decreases, and

the outer surface of shell has the lowest number of GPLs. The equal weight fraction for different GPL distributions may be estimated as follows [57,58].

$$\begin{aligned}
 U - GPLRC \quad V_{GPL}^{(k)} &= V_{GPL}^* \\
 X - GPLRC \quad V_{GPL}^{(k)} &= 4 V_{GPL}^* (0.5 + |K - (N_L + 1)/2|) / (2 + N_L) \\
 O - GPLRC \quad V_{GPL}^{(k)} &= 4 V_{GPL}^* ((N_L + 1)/2 - |K - (N_L + 1)/2|) \\
 A - GPLRC \quad V_{GPL}^{(k)} &= 2 V_{GPL}^* K / (N_L + 1)
 \end{aligned} \tag{1}$$

Here, V_{GPL}^K represents the volume content of GPLs in each layer of the shell panel. In Equation (1), K will change from 1 to N_L . V_{GPL}^K shows the volume fraction of nanofillers in the shell, and may be evaluated as follows [59]:

$$V_{GPL}^* = \frac{\Delta_{GPL} \rho_m}{\Delta_{GPL} \rho_m + \rho_{GPL} - \Delta_{GPL} \rho_{GPL}} \tag{2}$$

where in the above equation, ρ_{GPL} and ρ_m are the mass density of the nanofillers and polymeric matrix, respectively, and Δ_{GPL} is the weight fraction of the nanofillers. It is mentioned that due to the prevention of agglomeration phenomena, the maximum amount of Δ_{GPL} should be lower than 1%.

Based on the Halpin–Tsai micromechanics estimation [60–63], Young’s modulus of the shell panel is described as the following relations:

$$E = \frac{3}{8} \left(\frac{1 + \epsilon_L^{GPL} \eta_L^{GPL} V_{GPL}}{1 - \eta_L^{GPL} V_{GPL}} \right) E_m + \frac{5}{8} \left(\frac{1 + \epsilon_W^{GPL} \eta_W^{GPL} V_{GPL}}{1 - \eta_W^{GPL} V_{GPL}} \right) E_m \tag{3}$$

$$\epsilon_L^{GPL} = \frac{2l_{GPL}}{t_{GPL}} \tag{4}$$

$$\epsilon_w^{GPL} = \frac{2w_{GPL}}{t_{GPL}} \tag{5}$$

$$\eta_L^{GPL} = \frac{E_{GPL} - E_m}{E_{GPL} + \epsilon_L^{GPL} E_m} \tag{6}$$

$$\eta_W^{GPL} = \frac{E_{GPL} - E_m}{E_{GPL} + \epsilon_W^{GPL} E_m} \tag{7}$$

where E_{GPL} and E_m are the Young’s modulus of elasticity of the nanofillers and matrix, respectively. Additionally, l_{GPL} , w_{GPL} , t_{GPL} and V_{GPL} are the length, width, thickness and the volume fraction of the nanofillers, respectively. The rule of mixture estimation is employed to evaluate the Poisson’s ratio and the mass density of the GPL-RC [64,65]:

$$\rho = \rho_{GPL} V_{GPL} + \rho_m (1 - V_{GPL}) \tag{8}$$

$$\nu = \nu_{GPL} V_{GPL} + \nu_m (1 - V_{GPL}) \tag{9}$$

where ν_{GPL} and ν_m are the Poisson’s ratio of the nanofillers and matrix, respectively. The shear modulus, G , of the shell part is expressed as below [66–70]:

$$G = \frac{E}{2(1 + \nu)} \tag{10}$$

2.2. Governing Equations (FSDT—Virtual Work Principle)

In this section, FSDT is considered to describe the displacement components. Additionally, Lekhnitsky’s smeared stiffener assumptions are employed to present the relation between the shell panel with its rings and stringers. In this theory, the transverse normal

values at the mid-plane of the plate remain straight and rotate such that they do not remain perpendicular to the mid-surface after deformation. Applying the FSDT of the shells, the displacement constituents of the shell are considered to be as follows [71]:

$$\begin{aligned} u(x, \theta, z, t) &= u_0(x, \theta, t) + z \varphi_x(x, \theta, t) \\ v(x, \theta, z, t) &= v_0(x, \theta, t) + z \varphi_\theta(x, \theta, t) \\ w(x, \theta, z, t) &= w_0(x, \theta, t) \end{aligned} \tag{11}$$

where $u_0, v_0,$ and w_0 are the displacement components of the mid-plane of the shell panel along the axial, circumferential and radial directions, respectively. Additionally, $\varphi_x(x, \theta, t)$ and $\varphi_\theta(x, \theta, t)$ are the rotations of the mid-plane of the shell around the θ and x axes, respectively. Additionally, according to the FSDT, the kinematic relations are as follows:

$$\begin{aligned} \epsilon_x &= \epsilon_x^0 + z k_x \\ \epsilon_\theta &= \epsilon_\theta^0 + z k_\theta \\ \gamma_{x\theta} &= \gamma_{x\theta}^0 + z k_{x\theta} \\ \gamma_{\theta z} &= \gamma_{\theta z}^0 \\ \gamma_{xz} &= \gamma_{xz}^0 \end{aligned} \tag{12}$$

where

$$\begin{aligned} \epsilon_x^0 &= \frac{\partial u_0}{\partial x}; & k_x &= \frac{\partial \varphi_x}{\partial x}; & \epsilon_\theta^0 &= \frac{\partial v_0}{R \partial \theta} + \frac{w_0}{R}; \\ k_\theta &= \frac{\partial \varphi_\theta}{R \partial \theta}; & \gamma_{x\theta}^0 &= \frac{\partial u_0}{R \partial \theta} + \frac{\partial v_0}{\partial x}; & k_{x\theta} &= \frac{\partial \varphi_x}{R \partial \theta} + \frac{\partial \varphi_\theta}{\partial x}; \\ \gamma_{\theta z} &= \varphi_\theta + \frac{\partial w_0}{R \partial \theta} - \frac{v_0}{R}; & \gamma_{xz}^0 &= \varphi_x + \frac{\partial w_0}{\partial x}; \end{aligned} \tag{13}$$

According to the Lekhnitsky approach, the resultant force and moments for the FG-GPL cylindrical shell panel with stiffeners are considered as follows [72]:

$$\begin{aligned} N_x &= (A_{11} + \frac{E_s A_s}{s_s}) \epsilon_x^0 + A_{12} \epsilon_\theta^0 + (B_{11} + \frac{E_s A_s z_s}{s_s}) k_x + B_{12} k_\theta \\ N_\theta &= A_{12} \epsilon_x^0 + (A_{22} + \frac{E_r A_r}{s_r}) \epsilon_\theta^0 + B_{12} k_x + (B_{22} + \frac{E_r A_r z_r}{s_r}) k_\theta \\ N_{x\theta} &= A_{66} \gamma_{x\theta}^0 + B_{66} k_{x\theta} \\ M_x &= (B_{11} + \frac{E_s A_s z_s}{s_s}) \epsilon_x^0 + B_{12} \epsilon_\theta^0 + (D_{11} + \frac{E_s I_s}{s_s}) k_x + D_{12} k_\theta \\ M_\theta &= B_{12} \epsilon_x^0 + (B_{22} + \frac{E_r A_r z_r}{s_r}) \epsilon_\theta^0 + D_{12} k_x + (D_{22} + \frac{E_r I_r}{s_r}) k_\theta \\ M_{x\theta} &= B_{66} \gamma_{x\theta}^0 + D_{66} k_{x\theta} \\ \begin{cases} Q_\theta &= k_s (A_{44} + \frac{G_r A_r}{s_r}) \gamma_{\theta z} \\ Q_x &= k_s (A_{55} + \frac{G_s A_s}{s_s}) \gamma_{xz} \end{cases} \end{aligned} \tag{14}$$

where

$$\begin{aligned} A_{11} = A_{22} &= \int_{-\frac{h}{2}}^{\frac{h}{2}} \frac{E}{1-v^2} dz; & B_{11} = B_{22} &= \int_{-\frac{h}{2}}^{\frac{h}{2}} \frac{E}{1-v^2} z dz; & D_{11} = D_{22} &= \int_{-\frac{h}{2}}^{\frac{h}{2}} \frac{E}{1-v^2} z^2 dz; \\ A_{12} &= \int_{-\frac{h}{2}}^{\frac{h}{2}} \frac{vE}{1-v^2} dz; & B_{12} &= \int_{-\frac{h}{2}}^{\frac{h}{2}} \frac{vE}{1-v^2} z dz; & D_{12} &= \int_{-\frac{h}{2}}^{\frac{h}{2}} \frac{vE}{1-v^2} z^2 dz; \\ A_{66} &= \int_{-\frac{h}{2}}^{\frac{h}{2}} \frac{E}{2[1+v]} dz; & B_{66} &= \int_{-\frac{h}{2}}^{\frac{h}{2}} \frac{E}{2[1+v]} z dz; & D_{66} &= \int_{-\frac{h}{2}}^{\frac{h}{2}} \frac{E}{2[1+v]} z^2 dz; \\ A_{44} = A_{55} &= \int_{-\frac{h}{2}}^{\frac{h}{2}} \frac{E}{2[1+v]} dz; \\ I_s &= \frac{b_s h_s^3}{12} + A_s z_s^2; & I_r &= \frac{b_r h_r^3}{12} + A_r z_r^2; & z_s &= \pm \frac{h_s+h}{2}; & z_r &= \pm \frac{h_r+h}{2} \end{aligned} \tag{15}$$

The elasticity and the rigidity modulus of the stringers and the rings are defined as E_s and G_s , and E_r and G_r , respectively. The joints between the stiffeners (ribs and stringers) and the cylindrical shell panel are considered continuously and the cylindrical panel and stiffeners including the rings and stringers are made of the same material. It is mentioned that for the Lekhnitsky approach, the original structure and stiffeners can be manufactured integrally. Additionally, for the rings and stringers, the uniaxial state of stress is considered. $k_s = 5/6$ is the shear correction factor. Additionally, the height and width of the rings and stringers are considered as follows: h_r and b_r , and h_s and b_s , respectively. The areas of cross-section of the stringers and rings are denoted by A_s and A_r , respectively. In addition, the distances between two adjacent stringers and each ring are denoted by S_s and S_r , respectively; the distances between the centroid of an individual stringer and ring from the mid-surface of the shell panel are indicated by z_s and z_r , respectively. The forces and moments resultants in matrix form are as follows:

$$\begin{aligned} \begin{Bmatrix} N_x \\ N_\theta \\ N_{x\theta} \\ M_x \\ M_\theta \\ M_{x\theta} \end{Bmatrix} &= \begin{bmatrix} \bar{A}_{11} & \bar{A}_{12} & 0 & \bar{B}_{11} & \bar{B}_{12} & 0 \\ \bar{A}_{12} & \bar{A}_{22} & 0 & \bar{B}_{12} & \bar{B}_{22} & 0 \\ 0 & 0 & \bar{A}_{66} & 0 & 0 & \bar{B}_{66} \\ \bar{B}_{11} & \bar{B}_{12} & 0 & \bar{D}_{11} & \bar{D}_{12} & 0 \\ \bar{B}_{12} & \bar{B}_{22} & 0 & \bar{D}_{12} & \bar{D}_{22} & 0 \\ 0 & 0 & \bar{B}_{66} & 0 & 0 & \bar{D}_{66} \end{bmatrix} \begin{Bmatrix} \epsilon_x^0 \\ \epsilon_\theta^0 \\ \gamma_{x\theta}^0 \\ k_x \\ k_\theta \\ k_{x\theta} \end{Bmatrix}, \\ \begin{Bmatrix} Q_\theta \\ Q_x \end{Bmatrix} &= k_s \begin{bmatrix} \bar{A}_{44} & 0 \\ 0 & \bar{A}_{55} \end{bmatrix} \begin{Bmatrix} \gamma_{\theta z} \\ \gamma_{xz} \end{Bmatrix} \\ \bar{A} &= \begin{bmatrix} \bar{A}_{11} & \bar{A}_{12} & 0 \\ \bar{A}_{12} & \bar{A}_{22} & 0 \\ 0 & 0 & \bar{A}_{66} \end{bmatrix}, \\ \bar{B} &= \begin{bmatrix} \bar{B}_{11} & \bar{B}_{12} & 0 \\ \bar{B}_{12} & \bar{B}_{22} & 0 \\ 0 & 0 & \bar{B}_{66} \end{bmatrix}, \\ \bar{D} &= \begin{bmatrix} \bar{D}_{11} & \bar{D}_{12} & 0 \\ \bar{D}_{12} & \bar{D}_{22} & 0 \\ 0 & 0 & \bar{D}_{66} \end{bmatrix}, \bar{e} = k_s \begin{bmatrix} \bar{A}_{44} & 0 \\ 0 & \bar{A}_{55} \end{bmatrix} \end{aligned} \tag{16}$$

$$\begin{aligned} \bar{A}_{11} &= A_{11} + \frac{E_s A_s}{s_s}; & \bar{A}_{12} &= A_{12}; & \bar{A}_{22} &= A_{22} + \frac{E_r A_r}{s_r}; & \bar{A}_{66} &= A_{66}; \\ \bar{A}_{44} &= A_{44} + \frac{G_r A_r}{s_r}; & \bar{A}_{55} &= A_{55} + \frac{G_s A_s}{s_s}; \\ \bar{B}_{11} &= B_{11} + \frac{E_s A_s z_s}{s_s}; & \bar{B}_{12} &= B_{12}; \\ \bar{B}_{22} &= B_{22} + \frac{E_r A_r z_r}{s_r}; & \bar{B}_{66} &= B_{66} \\ \bar{D}_{11} &= D_{11} + \frac{E_s I_s}{s_s}; & \bar{D}_{12} &= D_{12}; \\ \bar{D}_{22} &= D_{22} + \frac{E_r I_r}{s_r}; & \bar{D}_{66} &= D_{66} \end{aligned}$$

For extending the governing equations of the shell panel, the virtual work principle is employed:

$$\int_0^t (\delta K - \delta U) dt = 0 \tag{17}$$

$$K = \frac{1}{2} \int_s \left[\int_{-\frac{h}{2}}^{\frac{h}{2}} \rho_{eq} (\dot{u} + \dot{v} + \dot{w}) dz \right] R d\theta dx,$$

$$U = \frac{1}{2} \int_s \left[N_x \epsilon_x^0 + N_\theta \epsilon_\theta^0 + N_{x\theta} \gamma_{x\theta}^0 + M_x k_x + M_\theta k_\theta + M_{x\theta} k_{x\theta} + Q_\theta \gamma_{\theta z} + Q_x \gamma_{xz} \right] R d\theta dx,$$

$$\rho_{eq} = \rho_{Sh} + \left(\frac{A_s}{s_s h}\right)\rho_s + \left(\frac{A_r}{s_r h}\right)\rho_r$$

where K is the kinetic energy of the structure and U is the strain energy. Additionally, ρ_{Sh} , ρ_s and ρ_r are the mass density of the shell, rings and stringers, respectively, and can be evaluated using Equation (8). The variation of kinetic energy is as follows:

$$\delta K = \int_s \left[\int_{-\frac{h}{2}}^{\frac{h}{2}} \rho_{eq} (\ddot{u} \delta u + \ddot{v} \delta v + \ddot{w} \delta w) dz \right] R d\theta dx, \tag{18}$$

where

$$\begin{cases} \delta u = \delta u_0 + z \delta \varphi_x \\ \delta v = \delta v_0 + z \delta \varphi_\theta \\ \delta w = \delta w_0 \end{cases} \quad \begin{cases} \ddot{u} = \frac{\partial^2 u_0}{\partial t^2} + z \frac{\partial^2 \varphi_x}{\partial t^2} \\ \ddot{v} = \frac{\partial^2 v_0}{\partial t^2} + z \frac{\partial^2 \varphi_\theta}{\partial t^2} \\ \ddot{w} = \frac{\partial^2 w_0}{\partial t^2} \end{cases} \tag{19}$$

$$\delta K = \int \int_{-\frac{h}{2}}^{\frac{h}{2}} \rho_{eq} \left(\left(\frac{\partial^2 u_0}{\partial t^2} + z \frac{\partial^2 \varphi_x}{\partial t^2} \right) (\delta u_0 + z \delta \varphi_x) + \left(\frac{\partial^2 v_0}{\partial t^2} + z \frac{\partial^2 \varphi_\theta}{\partial t^2} \right) (\delta v_0 + z \delta \varphi_\theta) + \frac{\partial^2 w_0}{\partial t^2} \delta w_0 \right) R dz d\theta dx$$

The strain energy for the stiffened FG-GPL multilayer cylindrical shell panel is presented as

$$U = \iint \left\{ N_x \varepsilon_x^0 + N_\theta \varepsilon_\theta^0 + N_{x\theta} \gamma_{x\theta}^0 + M_x K_x + M_\theta K_\theta + M_{x\theta} K_{x\theta} + Q_x \gamma_{xz} + Q_\theta \gamma_{\theta z} \right\} R dx d\theta \tag{20}$$

Equation (20) may be presented in the following matrix form:

$$U = \left([N_x, N_\theta, N_{x\theta}] \begin{bmatrix} \varepsilon_x^0 \\ \varepsilon_\theta^0 \\ \gamma_{x\theta}^0 \end{bmatrix} + [M_x, M_\theta, M_{x\theta}] \begin{bmatrix} K_x \\ K_\theta \\ K_{x\theta} \end{bmatrix} + [Q_x, Q_\theta] \begin{bmatrix} \gamma_{xz} \\ \gamma_{\theta z} \end{bmatrix} \right) R dx d\theta \tag{21}$$

Additionally, the kinematic relations (Equations (12) and (13)) may be presented in the following matrix form:

$$\begin{aligned} \begin{bmatrix} \varepsilon_x \\ \varepsilon_\theta \\ \gamma_{x\theta} \end{bmatrix} &= \begin{bmatrix} \varepsilon_x^0 \\ \varepsilon_\theta^0 \\ \gamma_{x\theta}^0 \end{bmatrix} + Z \begin{bmatrix} K_x \\ K_\theta \\ K_{x\theta} \end{bmatrix} = \begin{bmatrix} \frac{\partial}{\partial x} & 0 & 0 & Z \frac{\partial}{\partial x} & 0 \\ 0 & \frac{1}{R} \frac{\partial}{\partial \theta} & \frac{1}{R} & 0 & Z \frac{1}{R} \frac{\partial}{\partial \theta} \\ \frac{1}{R} \frac{\partial}{\partial \theta} & \frac{\partial}{\partial x} & 0 & Z \frac{1}{R} \frac{\partial}{\partial \theta} & Z \frac{\partial}{\partial x} \end{bmatrix} \begin{bmatrix} U_0 \\ V_0 \\ W_0 \\ \varphi_x \\ \varphi_\theta \end{bmatrix} = d_1 Q \\ \begin{bmatrix} \gamma_{xz}^0 \\ \gamma_{\theta z}^0 \end{bmatrix} &= \begin{bmatrix} 0 & 0 & \frac{\partial}{\partial x} & 1 & 0 \\ 0 & \frac{-1}{R} & \frac{1}{R} \frac{\partial}{\partial \theta} & 0 & 1 \end{bmatrix} \begin{bmatrix} U_0 \\ V_0 \\ W_0 \\ \varphi_x \\ \varphi_\theta \end{bmatrix} = d_2 Q, \quad \begin{bmatrix} \varepsilon_x^0 \\ \varepsilon_\theta^0 \\ \gamma_{x\theta}^0 \end{bmatrix} = \begin{bmatrix} \frac{\partial}{\partial x} & 0 & 0 & 0 & 0 \\ 0 & \frac{1}{R} \frac{\partial}{\partial \theta} & \frac{1}{R} & 0 & 0 \\ \frac{1}{R} \frac{\partial}{\partial \theta} & \frac{\partial}{\partial x} & 0 & 0 & 0 \end{bmatrix} \begin{bmatrix} U_0 \\ V_0 \\ W_0 \\ \varphi_x \\ \varphi_\theta \end{bmatrix} = d_3 Q \tag{22} \\ \begin{bmatrix} K_x \\ K_\theta \\ K_{x\theta} \end{bmatrix} &= \begin{bmatrix} 0 & 0 & 0 & \frac{\partial}{\partial x} & 0 \\ 0 & 0 & 0 & 0 & \frac{1}{R} \frac{\partial}{\partial \theta} \\ 0 & 0 & 0 & \frac{1}{R} \frac{\partial}{\partial \theta} & \frac{\partial}{\partial x} \end{bmatrix} \begin{bmatrix} U_0 \\ V_0 \\ W_0 \\ \varphi_x \\ \varphi_\theta \end{bmatrix} = d_4 Q \quad Q = \begin{bmatrix} U_0 \\ V_0 \\ W_0 \\ \varphi_x \\ \varphi_\theta \end{bmatrix} \end{aligned}$$

Hence, by substituting Equation (22) into (21), the strain energy can be expressed as follows:

$$\delta U = \int \left(\left((d_3 Q)^T \bar{A}^T + (d_4 Q)^T \bar{B}^T \right) (d_3 \delta Q) + \left((d_3 Q)^T \bar{B}^T + (d_4 Q)^T \bar{D}^T \right) (d_4 \delta Q) + (d_2 Q)^T \bar{e}^T (d_2 \delta Q) \right) R dx d\theta \tag{23}$$

3. Finite Element Modeling

FEM as a numerical solution is employed to solve the governing equations of the stiffened FG-GPL multilayer cylindrical shell panel. A two-dimensional four-noded element with 20 DOFs is used to discretize the shell panel. Additionally, a local-coordinate system (ξ, η) across the x and θ axes is employed for the shape functions.

The global and natural coordinates are related via the following relations [73]:

$$\xi = \frac{2(x - x_c)}{L^{(e)}} \quad \eta = \frac{2(\theta - \theta_c)}{\beta^{(e)}} \tag{24}$$

where $-1 \leq \xi, \eta \leq 1$ are along the x and θ axes, respectively. $L^{(e)}$ and $\beta^{(e)}$ are the length and span angle of each element, respectively. Additionally, θ_c and x_c are the circumferential and axial coordinates of the center of each element. The approximation functions in terms of the natural coordinates and the displacement components of each element are presented as follows:

$$\begin{aligned} \begin{Bmatrix} \Psi_1 \\ \Psi_2 \\ \Psi_3 \\ \Psi_4 \end{Bmatrix} &= \frac{1}{4} \begin{Bmatrix} (1 + \xi)(1 - \eta) \\ (1 + \xi)(1 + \eta) \\ (1 - \xi)(1 + \eta) \\ (1 - \xi)(1 - \eta) \end{Bmatrix} \tag{25} \\ \left(\begin{pmatrix} \Psi_1 & \dots & 0 \\ \vdots & \ddots & \vdots \\ 0 & \dots & \Psi_1 \end{pmatrix} \dots \begin{pmatrix} \Psi_4 & \dots & 0 \\ \vdots & \ddots & \vdots \\ 0 & \dots & \Psi_4 \end{pmatrix} \right) \begin{Bmatrix} u_{01} \\ v_{01} \\ w_{01} \\ \varphi_{x1} \\ \varphi_{\theta 1} \\ \vdots \\ u_{04} \\ v_{04} \\ w_{04} \\ \varphi_{x4} \\ \varphi_{\theta 4} \end{Bmatrix} &= \Psi q^{(e)} \end{aligned}$$

where $\Psi_n, n = 1, 2, 3, 4$ are the components of the shape functions, and Ψ is the matrix of the shape functions. $u_{0i}, v_{0i}, w_{0i}, \varphi_{xi}$ and $\varphi_{\theta i}$ are the nodal DOFs and are estimated as

$$\begin{aligned} u_0 &= \sum_{i=1}^4 \Psi_i U_{0i} \quad v_0 = \sum_{i=1}^4 \Psi_i V_{0i} \quad w_0 = \sum_{i=1}^4 \Psi_i W_{0i} \\ \varphi_x &= \sum_{i=1}^4 \Psi_i \theta_{xi} \quad \varphi_\theta = \sum_{i=1}^4 \Psi_i \theta_{\theta i} \end{aligned} \tag{26}$$

Substituting Equation (26) into Equations (19) and (23), the Hamilton’s principle in Equation (17) can be rewritten as below.

$$\begin{aligned} \int_{\Omega_0^e} &\left[\left((d_3 \Psi)^T \bar{A}^T (d_3 \Psi) + (d_4 \Psi)^T \bar{B}^T (d_3 \Psi) + (d_3 \Psi)^T \bar{B}^T (d_4 \Psi) \right. \right. \\ &\left. \left. + (d_4 \Psi)^T \bar{D}^T (d_4 \Psi) + (d_2 \Psi)^T \bar{e}^T d_2 \Psi \right) q^{(e)} + \Psi^T I \Psi \ddot{q}^{(e)} \right] R dx d\theta = 0 \\ I &= \begin{bmatrix} I_0 & 0 & 0 & I_1 & 0 \\ 0 & I_0 & 0 & 0 & I_1 \\ 0 & 0 & I_0 & 0 & 0 \\ I_1 & 0 & 0 & I_2 & 0 \\ 0 & I_1 & 0 & 0 & I_2 \end{bmatrix}, \quad \begin{Bmatrix} I_0 \\ I_1 \\ I_2 \end{Bmatrix} = \int_{-\frac{h}{2}}^{\frac{h}{2}} \begin{Bmatrix} 1 \\ z \\ z^2 \end{Bmatrix} \rho_{eq} dz \end{aligned} \tag{27}$$

Additionally, by replacing $d_2 \Psi = B_2, d_3 \Psi = B_3, d_4 \Psi = B_4$ in Equation (27), and by sorting it, Equation (28) is derived for a cylindrical panel element:

$$(k_1 + k_2 + k_3)^{(e)} q^{(e)} + M^{(e)} \ddot{q}^{(e)} = 0 \tag{28}$$

where

$$\begin{aligned}
 M^e &= \int_{\Omega_0^e} \Psi^T I \Psi R \, dx \, d\theta \\
 k_1^e &= \int \left[B_3^T \bar{A}^T + B_4^T \bar{B}^T B_3 \right] R \, dx \, d\theta \\
 k_2^e &= \int \left[B_3^T \bar{B}^T B_4 + B_4^T \bar{D}^T B_4 \right] R \, dx \, d\theta. \\
 k_3^e &= \int \left[B_2^T \bar{e}^T B_2 \right] R \, dx \, d\theta
 \end{aligned}
 \tag{29}$$

After evaluating the element matrices of each element, and via the summation of these matrices, the finite element model of the stiffened FG-GPL multilayer cylindrical panel is as follows

$$(k_1 + k_2 + k_3)q + M\ddot{q} = 0
 \tag{30}$$

Finally, for the free vibration problem, the following eigenvalue problem is considered.

$$\left((k_1 + k_2 + k_3) - M\omega^2 \right) q = 0
 \tag{31}$$

where in Equation (31), ω represents the circular natural frequencies of the stiffened shell panel and q is its mode shapes.

The details of the solution procedure for the free vibration problem (Equation (31)) are as follows:

1. Calculating the stiffness and mass matrices of each element according to Equation (29);
2. Assembling the stiffness and mass matrices of each element to obtain the final stiffness and mass matrices of the shell;
3. Applying the Sparse command on the matrices to reduce the size of matrices and also the computation time;
4. Applying displacement boundary conditions on the Sparse matrices according to Equation (32);
5. Solving the eigenvalue problem (Equation (31)) to obtain the natural frequencies and mode shapes. To solve Equation (31) in Matlab software, the command `eigs(k1 + k2 + k3, M; number of desired mode shapes, 0)` is used. Briefly, 0 means that the lowest natural frequency close to 0 is desired. In this study, number of desired mode shapes = 6.

In this study, the following displacement boundary conditions for a cylindrical panel are considered:

When all edges of the cylindrical shell panel are clamped (CCCC), the following can be observed :

$$u_0, v_0, w_0, \varphi_x, \varphi_\theta = 0 \quad \text{at } (x = 0, \theta), (x = L, \theta), (x, \theta = 0), (x, \theta = \beta)$$

Additionally, when all edges of the structure are simply supported (SSSS) :

$$\begin{aligned}
 u_0, w_0 &= 0 & \text{at } (x = 0, \theta), (x = L, \theta) \\
 v_0, w_0 &= 0 & \text{at } (x, \theta = 0), (x, \theta = \beta)
 \end{aligned}
 \tag{32}$$

4. Numerical Results and Discussion

4.1. Verification of Results

The vibration analysis of a stiffened cylindrical panel reinforced by a graphene platelet has not been investigated so far. Hence, for verification purposes, numerical results are derived for a homogenous stiffened cylindrical panel with a ring and stringer for free-boundary conditions. For this target, the weight fraction of GPLs in the present study should be considered zero. Additionally, the geometries and mechanical properties of the cylindrical panel of Ref [8] are considered ($E = 209 \text{ GPa}$, $\nu = 0.3$, $\rho = 7800 \text{ kg/m}^3$). Then, the natural frequencies of the cylindrical panel with rings and stringers are obtained and compared with those obtained by Samanta and Mukhopadhyay [8]. This comparison is given in Table 1 and shows excellent agreement. In [8], a flat shell element with a combination of a DKT (discrete Kirchhoff's triangle) plate-bending element and Allman's plane stress triangle is employed to model the problem. The bending element was a six-noded triangle with 12 degrees of freedom, while in the present study, FSDT with four-

noded shell element is used. Hence, the difference between the present results and those of the reference is related to the different theories that are employed in this investigation and that of Samanta and Mukhopadhyay [8].

Table 1. A comparison of the natural frequencies of a stiffened shell between the present results and those of the reference Samanta and Mukhopadhyay [8].

Natural Frequencies (Hz)	ω_1	ω_2	ω_3	ω_4	ω_5	ω_6
Samanta and Mukhopadhyay [8]	144	247	374	559	593	678
(Present)	138	241	369	554	587	669

4.2. Numerical Results

In this section, the first six natural frequencies of the stiffened multilayer cylindrical panel reinforced by GPLs are presented. The influences of various parameters including four different patterns of the GPLs for the shell panel, rings and stringers, various weight fractions of GPLs, two different boundary conditions and various numbers of the ring and stringer on the free vibration response of the structure are examined. The geometries and mechanical properties of the stiffened FG-GPL multilayer cylindrical panel are assumed to be as follows:

Mechanical property:

$E_m = 3 \text{ GPa}$, $\rho_m = 1200 \text{ kg/m}^3$, $\nu_m = 0.34$ for epoxy, and $E_{GPL} = 1.01 \text{ TPa}$, $\rho_{GPL} = 1062.5 \text{ kg/m}^3$, $\nu_{GPL} = 0.186$, $w_{GPL} = 1.5 \text{ }\mu\text{m}$, $l_{GPL} = 2.5 \text{ }\mu\text{m}$, $t_{GPL} = 1.5 \text{ nm}$ for GPLs.

- (a) Geometry of the cylindrical panel: $L = 2$, $R = 0.5$, $\theta = 120^\circ$
- (b) Geometry of the rings and stringers: $h_s = 0.02$, $b_s = 0.04$, $h_r = 0.02$, $b_r = 0.04$

The convergence of the finite element results of the present research is investigated through comparing the results of the successive refinement of the element size. In this regard, results are compared for meshes with an adequate fixed number of elements along the θ axis but with various numbers of elements in the axial direction. Table 2 demonstrates that applying 50×30 elements through the (n_x, n_θ) direction is enough to obtain convergent results.

Table 2. Convergence study of the fundamental natural frequency for the stiffened cylindrical panel structure (SSSS boundary condition; $S_s = 0.378$, $S_r = 0.5$, $\Delta = 1 \text{ wt. } \%$, GPL X for the structure, and GPL O for rings and stringers).

Number of Elements for Structure (n_x, n_θ)	30×30	40×30	50×30
ω_1	326.82	312.24	310.32

The influences of the various GPL patterns for the cylindrical panel shell and the rings and stringers on the natural frequencies of the structure are given in Table 3 (SSSS boundary condition; $S_s = 0.378$, $S_r = 0.5$, $N_r = N_s = 5$, and $\Delta = 1 \text{ wt. } \%$). As can be seen from this table, the pattern of GPLX for the cylindrical panel shell in conjunction with GPLX for the ring and stringer has the highest number of natural frequencies of the structure among various GPL patterns for the cylindrical panel, ring and stringer while the pattern of GPLUD for the cylindrical panel shell in conjunction with GPLUD for the rings and stringer has the lowest number of natural frequencies. These differences are approximately 60% and can be useful for engineers in their design. On the other hand, when the concentration of the nano-fillers on the top and bottom of the structure is more than in the middle, the structure will be accorded more rigidity and stiffness. Additionally, for each pattern of reinforcement of the cylindrical shell panel, the maximum and minimum natural frequencies belong to the shells when their rings and stringers are reinforced with the GPLX distribution and

GPLUD, respectively. Additionally, the effect of reinforcing the shell panel with GPLs on the overall stiffness of the structure is more dominant than that in the case where the rings and stringers are reinforced by GPLs. Furthermore, in each pattern of reinforcement for the cylindrical shell panel except for GPL-UD, the numbers of natural frequencies of the structure are close to each other when the reinforcement of the rings and stringers is GPL-O and GPL-A. The effect of various weight fractions of GPLs on the natural frequencies of the structure is depicted in Table 4. In this case, the patterns of reinforcement for the shell panel, rings and stringers are the same. By increasing the weight fraction of nano-fillers (from 0 to 0.01) for different GPL patterns, the number of natural frequencies of the structure significantly increases (by approximately 118% for the GPL-X pattern). The influence of increasing the weight fraction of the nano-fillers on the number of natural frequencies of the structure for GPL-X is greater than that of the other patterns while the impact of increasing the weight fraction of the nano-fillers on the number of natural frequencies of the structure for GPL-UD is smaller than that of the other patterns. Table 5 shows the impact of various boundary conditions on the natural frequencies of the structure ($S_s = 0.378$, $S_r = 0.5$, $N_r = N_s = 5$, and $\Delta = 1$ wt. %). It is obvious from this table that the CCCC boundary condition has higher natural frequencies than does the SSSS boundary condition due to the fact that the CCCC boundary condition provides more rigidity than does the SSSS boundary condition. Table 6 indicates the influences of the number of rings and stringers on the natural frequencies of the stiffened cylindrical shell panel for two different boundary conditions (the GPLX pattern for the cylindrical panel; ring and stringer; $\Delta = 1$ wt. %). By increasing the number of rings and stringers, the natural frequencies are changed a little. It is interesting that the number of fundamental frequencies of the structure for the CCCC boundary condition is increased a little by increasing the number of rings and stringers while the number of the fundamental frequencies of the structure for the SSSS boundary condition is decreased a little by increasing the numbers of rings and stringers. On the other hand, stiffening the shell with a ring and stringer may decrease or increase the natural frequencies of the structure a little depending on the boundary condition.

Table 3. The influences of various GPL patterns for the cylindrical panel shell and ring and stringer on the natural frequencies (Hz) of the structure (SSSS boundary condition; $S_s = 0.378$, $S_r = 0.5$; $\Delta = 1$ wt. %).

GPL Pattern for Cylindrical Panel Shell	GPL Pattern for Ring and Stringer	ω_1	ω_2	ω_3	ω_4	ω_5	ω_6
GPL-UD	UD	225.13	374.82	435.39	452.77	465.65	592.43
	X	258.75	433.25	504.36	578.56	593.13	769.27
	O	242.31	420.88	499.98	524.44	560.05	673.14
	A	228.54	390.43	467.24	488.34	497.22	626.46
GPL-X	UD	282.76	479.21	539.81	599.99	633.12	710.47
	X	362.55	614.98	697.29	731.08	766.46	968.71
	O	310.32	550.74	642.12	675.84	700.48	893.65
	A	299.47	494.32	566.36	620.11	658.22	760.33
GPL-O	UD	240.88	390.15	470.46	506.42	525.84	631.26
	X	281.65	480.67	553.57	595.72	616.71	744.64
	O	276.18	466.74	549.34	588.07	600.39	730.12
	A	265.94	441.46	526.25	567.66	580.35	700.49

Table 3. Cont.

GPL Pattern for Cylindrical Panel Shell	GPL Pattern for Ring and Stringer	ω_1	ω_2	ω_3	ω_4	ω_5	ω_6
GPL-A	UD	226.83	362.49	432.72	450.24	478.55	600.06
	X	273.56	471.82	520.18	590.88	601.56	716.77
	O	233.14	420.13	500.72	541.57	550.22	680.48
	A	230.13	400.78	474.30	500.94	510.74	635.33

Table 4. The impact of different weight fractions of GPLs on the natural frequencies (Hz) of the structure (SSSS boundary condition; $S_s = 0.378$; $S_r = 0.5$).

GPL Pattern for Cylindrical Panel, Ring and Stringer	$\Delta_{GPL} \%$	ω_1	ω_2	ω_3	ω_4	ω_5	ω_6
GPL-X	0	166.66	277.03	322.22	347.9	355.28	438.51
	0.5	312.06	529.61	600.86	630.17	660.34	834.48
	1	362.55	614.98	697.29	731.08	766.46	968.71
GPL-A	0	166.66	277.03	322.22	347.9	355.28	438.51
	0.5	203.53	357.14	423.21	446.42	455.35	566.94
	1	230.13	400.78	474.30	500.94	510.74	635.33
GPL-UD	0	166.66	277.03	322.22	347.9	355.28	438.51
	0.5	187.55	311.66	378.26	400.12	420.18	493.33
	1	225.13	374.82	435.39	452.77	465.65	592.43
GPL-O	0	166.66	277.03	322.22	347.9	355.28	438.51
	0.5	230.47	391.59	473.27	498.30	500.42	634.78
	1	276.18	466.74	549.34	588.07	600.39	730.12

Table 5. The impact of various boundary conditions on the natural frequencies (Hz) of the structure ($S_s = 0.378$; $S_r = 0.5$; $\Delta = 1$ wt. %).

GPL Pattern for Cylindrical Panel, Ring and Stringer	Boundary Condition	ω_1	ω_2	ω_3	ω_4	ω_5	ω_6
GPL-X	cccc	696.26	912.85	1057.23	1145.3	1175.5	1289.4
	ssss	362.55	614.98	697.29	731.08	766.46	968.71
GPL-UD	cccc	421.96	557.72	647.13	702.76	720.33	793.83
	ssss	225.13	374.82	435.39	452.77	465.65	592.43
GPL-O	cccc	524.44	884.23	1032.75	1134.88	1140.55	1350.62
	ssss	276.18	466.74	549.34	588.07	600.39	730.12
GPL-A	cccc	391.63	700.45	860.27	930.18	969.31	1235.77
	ssss	230.13	400.78	474.30	500.94	510.74	635.33

Table 6. The impact of increasing the number of rings and stringers on the natural frequencies (Hz) of the structure (GPL-X for shell panel, ring and stringer, $\Delta = 1$ wt. %).

Boundary Condition	Number of Ring and Stringer	ω_1	ω_2	ω_3	ω_4	ω_5	ω_6
CCCC	Nr = Ns = 5	696.26	912.85	1057.23	1145.3	1175.5	1289.4
	Nr = Ns = 7	697.12	913.00	1053.84	1140.72	1176.02	1284.37
	Nr = Ns = 10	698.23	913.78	1049.6	1136.8	1177.6	1280
SSSS	Nr = Ns = 5	362.55	614.98	697.29	731.08	766.46	968.71
	Nr = Ns = 7	360.01	613.47	690.33	727.66	767.13	969.47
	Nr = Ns = 10	359.62	613.2	685.22	719.85	770.11	971.13

5. Conclusions

The natural frequencies of stiffened cylindrical shell panels reinforced with graphene platelets have been studied for the first time. Four GPL patterns including GPL-X, GPL-O, GPL UD, and GPL-A were considered along with the shell thickness of the cylindrical panel, rings and stringers. Based on first-order shear deformation theory and by employing FEM based on the Hamilton principle and the Rayleigh–Ritz method, the governing equations of the structure were obtained and solved. The influences of GPL patterns for the cylindrical panel, rings and stringers, the weight fraction of nanofillers, various boundary conditions and different numbers of stringers and rings on the natural frequencies of a stiffened cylindrical shell panel reinforced with a graphene platelet have been studied.

Remarkable findings which can be used in practical applications are as follows:

- (a) Maximum and minimum natural frequencies were related to GPL-X and GPL-UD, respectively;
- (b) The effect of reinforcing the shell panel with GPLs on the overall stiffness of the structure was more dominant than that in the case that the rings and stringers were reinforced by GPLs. The maximum influences of the GPL patterns and weight fraction of GPLs on the natural frequencies of the structure were approximately 60% and 118%, respectively;
- (c) By increasing the weight fraction of GPLs, the number of natural frequencies of the structure for the GPL-X pattern was increased to more than that of other GPL distributions;
- (d) The CCCC boundary condition had higher natural frequencies than did the SSSS boundary condition;
- (e) Reinforcement including rings and stringers may decrease or increase the natural frequencies of the structure depending on the boundary condition;
- (f) By increasing the number of rings and stringers, the natural frequencies were changed a little;
- (g) The influences of strengthening the shell with GPLs was much greater than that of stiffening it with rings and stringers.
- (h) In each pattern of reinforcement for the cylindrical shell panel except for GPL-UD, the numbers of natural frequencies of the structure were close to each other when the reinforcement of rings and stringers were considered to be GPL-O and GPL-A. This means that for these cases, they can be used interchangeably.

Author Contributions: Conceptualization, J.L.; Methodology, Y.Z. (Yuhua Zhou), Y.Z. (Yanhu Zhang), C.L. and M.B.; Software, Y.Z. (Yuhua Zhou), Y.Z. (Yanhu Zhang), B.N.C., J.L., C.L. and K.A.; Validation, Y.Z. (Yuhua Zhou), B.N.C. and K.A.; Formal analysis, Y.Z. (Yuhua Zhou) and Y.Z. (Yanhu Zhang); Investigation, Y.Z. (Yuhua Zhou), Y.Z. (Yanhu Zhang), B.N.C., C.L. and K.A.; Resources, C.L.; Writing—original draft, Y.Z. (Yuhua Zhou), Y.Z. (Yanhu Zhang) and B.N.C.; Writing—review & editing, J.L., C.L., M.B. and K.A.; Visualization, Y.Z. (Yanhu Zhang); Supervision, J.L. and M.B.; Project administration, J.L. and M.B. All authors have read and agreed to the published version of the manuscript.

Funding: This work was supported by Natural Science Research of Jiangsu Higher Education Institutions of China (no. 18KJB510007) and Senior Talent Foundation of Jiangsu University (no. 16JDG037).

Acknowledgments: This work was supported by Natural Science Research of Jiangsu Higher Education Institutions of China (no. 18KJB510007) and Senior Talent Foundation of Jiangsu University (no. 16JDG037).

Conflicts of Interest: The authors declare no conflict of interest.

References

1. Crenwelge, O.E., Jr.; Muster, D. Free vibrations of ring-and-stringer-stiffened conical shells. *J. Acoust. Soc. Am.* **1969**, *46*, 176–185. [[CrossRef](#)]
2. Nayak, A.N.; Satpathy, L.; Tripathy, P.K. Free vibration characteristics of stiffened plates. *Int. J. Adv. Struct. Eng.* **2018**, *10*, 153–167. [[CrossRef](#)]
3. Nayak, A.N.; Bandyopadhyay, J.N. Free Vibration of Laminated Composite Stiffened Shallow Shells. In *Toughened Composites*; CRC Press: Boca Raton, FL, USA, 2022; pp. 261–276.
4. Sinha, L.; Mishra, S.S.; Nayak, A.N.; Sahu, S.K. Free vibration characteristics of laminated composite stiffened plates: Experimental and numerical investigation. *Compos. Struct.* **2020**, *233*, 111557. [[CrossRef](#)]
5. Nayak, A.N.; Bandyopadhyay, J.N. Free vibration analysis and design aids of stiffened conoidal shells. *J. Eng. Mech.* **2022**, *128*, 419–427. [[CrossRef](#)]
6. Naghsh, A.; Saadatpour, M.M.; Azhari, M. Free vibration analysis of stringer stiffened general shells of revolution using a meridional finite strip method. *Thin Walled Struct.* **2015**, *94*, 651–662. [[CrossRef](#)]
7. Quoc, T.H.; Van Tham, V.; Tu, T.M. Free Vibration of Stiffened Functionally Graded Porous Cylindrical Shell Under Various Boundary Conditions. In *Modern Mechanics and Applications*; Springer: Singapore, 2022; pp. 347–361.
8. Samanta, A.; Mukhopadhyay, M. Free vibration analysis of stiffened shells by the finite element technique. *Eur. J. Mech. A Solids* **2004**, *23*, 159–179. [[CrossRef](#)]
9. Mustafa, B.A.J.; Ali, R. An energy method for free vibration analysis of stiffened circular cylindrical shells. *Comput. Struct.* **1989**, *32*, 355–363. [[CrossRef](#)]
10. Al-Najafi, A.M.J.; Warburton, G.B. Free vibration of ring-stiffened cylindrical shells. *J. Sound Vib.* **1970**, *13*, 9–25. [[CrossRef](#)]
11. Zarei, M.; Rahimi, G.H.; Hemmatnezhad, M. Free vibrational characteristics of grid-stiffened truncated composite conical shells. *Aerosp. Sci. Technol.* **2020**, *99*, 105717. [[CrossRef](#)]
12. Zarei, M.; Rahimi, G.H.; Hemmatnezhad, M. On the free vibrations of joined grid-stiffened composite conical-cylindrical shells. *Thin Walled Struct.* **2021**, *161*, 107465. [[CrossRef](#)]
13. Aris, H.; Ahmadi, H. Using the higher-order shear deformation theory to analyze the free vibration of stiffened rotating FGM conical shells in a thermal environment. *Thin Walled Struct.* **2023**, *183*, 110366. [[CrossRef](#)]
14. Ansari, E.; Hemmatnezhad, M.; Taherkhani, A. Free vibration analysis of grid-stiffened composite truncated spherical shells. *Thin Walled Struct.* **2023**, *182*, 110237. [[CrossRef](#)]
15. Tran, M.T.; Nguyen, V.L.; Pham, S.D.; Rungamornrat, J. Free vibration of stiffened functionally graded circular cylindrical shell resting on Winkler–Pasternak foundation with different boundary conditions under thermal environment. *Acta Mech.* **2020**, *231*, 2545–2564. [[CrossRef](#)]
16. Tuan, T.A.; Quoc, T.H.; Tu, T.M. Free vibration analysis of laminated stiffened cylindrical panels using finite element method. *Vietnam J. Sci. Technol.* **2016**, *54*, 771–784. [[CrossRef](#)]
17. Nguyen, V.L.; Hoang, T.P. Analytical solution for free vibration of stiffened functionally graded cylindrical shell structure resting on elastic foundation. *SN Appl. Sci.* **2019**, *1*, 1–12. [[CrossRef](#)]
18. Li, X.-Q.; Zhang, W.; Yang, X.-D.; Song, L.-K. A unified approach of free vibration analysis for stiffened cylindrical shell with general boundary conditions. *Math. Probl. Eng.* **2019**, *2019*, 4157930. [[CrossRef](#)]
19. Bich, D.H.; Van Dung, D.; Nam, V.H. Nonlinear dynamical analysis of eccentrically stiffened functionally graded cylindrical panels. *Compos. Struct.* **2012**, *94*, 2465–2473. [[CrossRef](#)]
20. Carrera, E.; Zappino, E.; Filippi, M. Free vibration analysis of thin-walled cylinders reinforced with longitudinal and transversal stiffeners. *J. Vib. Acoust.* **2013**, *135*, 011019. [[CrossRef](#)]
21. Lugovoi, P.Z.; Prokopenko, N.Y. Influence of reinforcement and elastic foundation on the vibrations of shallow shells with rectangular planform. *Int. Appl. Mech.* **2011**, *47*, 714–719. [[CrossRef](#)]
22. Shahani, A.R.; Kiarasi, F. Numerical and Experimental Investigation on Post-buckling Behavior of Stiffened Cylindrical Shells with Cutout subject to Uniform Axial Compression. *J. Appl. Comput. Mech.* **2023**, *9*, 25–44.
23. Rao, M.N.; Schmidt, R.; Schröder, K.U. Forced vibration analysis of FG-graphene platelet reinforced polymer composite shells bonded with piezoelectric layers considering electroelastic nonlinearities. In *Smart Materials, Adaptive Structures and Intelligent Systems*; Society of Mechanical Engineers: New York, NY, USA, 2018; Volume 51944, p. V001T03A006.
24. Van Do, V.N.; Lee, C.-H. Bézier extraction based isogeometric analysis for bending and free vibration behavior of multilayered functionally graded composite cylindrical panels reinforced with graphene platelets. *Int. J. Mech. Sci.* **2020**, *183*, 105744. [[CrossRef](#)]

25. Amirabadi, H.; Farhatnia, F.; Eftekhari, S.A.; Hosseini-Ara, R. Free vibration analysis of rotating functionally graded GPL-reinforced truncated thick conical shells under different boundary conditions. *Mech. Based Des. Struct. Mach.* **2020**, *50*, 3821–3852. [[CrossRef](#)]
26. Jamalabadi, M.Y.A.; Borji, P.; Habibi, M.; Pelalak, R. Nonlinear vibration analysis of functionally graded GPL-RC conical panels resting on elastic medium. *Thin Walled Struct.* **2021**, *160*, 107370. [[CrossRef](#)]
27. Salehi, M.; Gholami, R.; Ansari, R. Nonlinear Resonance of Functionally Graded Porous Circular Cylindrical Shells Reinforced by Graphene Platelet with Initial Imperfections Using Higher-Order Shear Deformation Theory. *Int. J. Struct. Stab. Dyn.* **2022**, *22*, 2250075. [[CrossRef](#)]
28. Yang, S.; Hao, Y.; Zhang, W.; Yang, L.; Liu, L. Nonlinear vibration of functionally graded graphene platelet-reinforced composite truncated conical shell using first-order shear deformation theory. *Appl. Math. Mech.* **2021**, *42*, 981–998. [[CrossRef](#)]
29. Van Do, V.N.; Lee, C.-H. Static bending and free vibration analysis of multilayered composite cylindrical and spherical panels reinforced with graphene platelets by using isogeometric analysis method. *Eng. Struct.* **2020**, *215*, 110682. [[CrossRef](#)]
30. Esmaeili, H.R.; Kiani, Y. Vibrations of graphene platelet reinforced composite doubly curved shells subjected to thermal shock. *Mech. Based Des. Struct. Mach.* **2022**, 1–30. [[CrossRef](#)]
31. Baghbadorani, A.A.; Kiani, Y. Free vibration analysis of functionally graded cylindrical shells reinforced with graphene platelets. *Compos. Struct.* **2021**, *276*, 114546. [[CrossRef](#)]
32. Dong, Y.; Zhu, B.; Wang, Y.; Li, Y.; Yang, J. Nonlinear free vibration of graded graphene reinforced cylindrical shells: Effects of spinning motion and axial load. *J. Sound Vib.* **2018**, *437*, 79–96. [[CrossRef](#)]
33. Dong, Y.; Li, X.; Gao, K.; Li, Y.; Yang, J. Harmonic resonances of graphene-reinforced nonlinear cylindrical shells: Effects of spinning motion and thermal environment. *Nonlinear Dyn.* **2020**, *99*, 981–1000. [[CrossRef](#)]
34. Song, J.; Karami, B.; Shahsavari, D.; Civalek, Ö. Wave dispersion characteristics of graphene reinforced nanocomposite curved viscoelastic panels. *Compos. Struct.* **2021**, *277*, 114648. [[CrossRef](#)]
35. Sobhani, E.; Masoodi, A.R.; Dimitri, R.; Tornabene, F. Free vibration of porous graphene oxide powder nano-composites assembled paraboloidal-cylindrical shells. *Compos. Struct.* **2023**, *304*, 116431. [[CrossRef](#)]
36. Zare, R.; Najaafi, N.; Habibi, M.; Ebrahimi, F.; Safarpour, H. Influence of imperfection on the smart control frequency characteristics of a cylindrical sensor-actuator GPLRC cylindrical shell using a proportional-derivative smart controller. *Smart Struct. Syst. Int. J.* **2020**, *26*, 469–480.
37. Rezaiee Pajand, M.; Sobhan, E.; Masoodi, A. Vibrational behavior of exponentially graded joined conical-conical shells. *Steel Compos. Struct.* **2022**, *43*, 603–623.
38. Sobhani, E.; Avcar, M. The influence of various nanofiller materials (CNTs, GNPs, and GOPs) on the natural frequencies of Nanocomposite Cylindrical Shells: A comparative study. *Mater. Today Commun.* **2022**, *33*, 104547. [[CrossRef](#)]
39. Sobhani, E.; Masoodi, A.R.; Ahmadi-Pari, A.R. Free-damped vibration analysis of graphene nano-platelet nanocomposite joined conical-conical-cylindrical shell marine-like structures. *Ocean. Eng.* **2022**, *261*, 112163. [[CrossRef](#)]
40. Sobhani, E.; Masoodi, A.R.; Ahmadi-Pari, A.R. Wave frequency responses estimate of the nanocomposite linked hemispherical-conical shell underwater-like bodies with the impacts of two types of graphene-based nanofillers. *Ocean Eng.* **2022**, *262*, 112329. [[CrossRef](#)]
41. Sobhani, E.; Masoodi, A.R.; Ahmadi-Pari, A.R. Circumferential vibration analysis of nano-porous-sandwich assembled spherical-cylindrical-conical shells under elastic boundary conditions. *Eng. Struct.* **2022**, *273*, 115094. [[CrossRef](#)]
42. Sobhani, E.; Masoodi, A.R.; Civalek, Ö. On vibrational-based numerical simulation of a jet engine cowl shell-like structure. *Mech. Adv. Mater. Struct.* **2022**, *30*, 4016–4027. [[CrossRef](#)]
43. Sobhani, E. On the vibrational analysis of combined paraboloidal-conical air vehicle segment shell-type structures. *Aerosp. Sci. Technol.* **2022**, *129*, 107823. [[CrossRef](#)]
44. Song, M.; Yang, J.; Kitipornchai, S.; Zhu, W. Buckling and postbuckling of biaxially compressed functionally graded multilayer graphene nanoplatelet-reinforced polymer composite plates. *Int. J. Mech. Sci.* **2017**, *131*, 345–355. [[CrossRef](#)]
45. Song, M.; Kitipornchai, S.; Yang, J. Free and forced vibrations of functionally graded polymer composite plates reinforced with graphene nanoplatelets. *Compos. Struct.* **2017**, *159*, 579–588. [[CrossRef](#)]
46. Wang, Y.Q.; Ye, C.; Zu, J.W. Nonlinear vibration of metal foam cylindrical shells reinforced with graphene platelets. *Aerosp. Sci. Technol.* **2019**, *85*, 359–370. [[CrossRef](#)]
47. Chai, Q.; Wang, Y.Q. Traveling wave vibration of graphene platelet reinforced porous joined conical-cylindrical shells in a spinning motion. *Eng. Struct.* **2022**, *252*, 113718. [[CrossRef](#)]
48. Ye, C.; Wang, Y.Q. Nonlinear forced vibration of functionally graded graphene platelet-reinforced metal foam cylindrical shells: Internal resonances. *Nonlinear Dyn.* **2021**, *104*, 2051–2069. [[CrossRef](#)]
49. Teng, M.W.; Wang, Y.Q. Nonlinear forced vibration of simply supported functionally graded porous nanocomposite thin plates reinforced with graphene platelets. *Thin Walled Struct.* **2021**, *164*, 107799. [[CrossRef](#)]
50. Wang, Y.; Wu, H.; Yang, F.; Wang, Q. An efficient method for vibration and stability analysis of rectangular plates axially moving in fluid. *Appl. Math. Mech.* **2021**, *42*, 291–308. [[CrossRef](#)]
51. Chai, Q.; Wang, Y.Q. A general approach for free vibration analysis of spinning joined conical-cylindrical shells with arbitrary boundary conditions. *Thin Walled Struct.* **2021**, *168*, 108243. [[CrossRef](#)]

52. Safarpour, M.; Rahimi, A.R.; Alibeigloo, A. Static and free vibration analysis of graphene platelets reinforced composite truncated conical shell, cylindrical shell, and annular plate using theory of elasticity and DQM. *Mech. Based Des. Struct. Mach.* **2020**, *48*, 496–524. [[CrossRef](#)]
53. Babaei, M.; Kiarasi, F.; Tehrani, M.S.; Hamzei, A.; Mohtarami, E.; Asemi, K. Three dimensional free vibration analysis of functionally graded graphene reinforced composite laminated cylindrical panel. *Proc. Inst. Mech. Eng. Part L J. Mater. Des. Appl.* **2022**, *236*, 1501–1514. [[CrossRef](#)]
54. Kiarasi, F.; Babaei, M.; Mollaei, S.; Mohammadi, M.; Asemi, K. Free vibration analysis of FG porous joined truncated conical-cylindrical shell reinforced by graphene platelets. *Adv. Nano Res.* **2021**, *11*, 361–380.
55. Zhang, D.; Wang, Y.; Li, L. Free Vibration Response of FG Porous Joined Hemispherical–Cylindrical–Hemispherical Shell Vessels Reinforced by Graphene Platelet. *Int. J. Struct. Stab. Dyn.* **2022**, *23*, 2350025. [[CrossRef](#)]
56. Zu, X.; Gao, Z.; Zhao, J.; Wang, Q.; Li, H. Vibration Suppression Performance of FRP Spherical–Cylindrical Shells with Porous Graphene Platelet Coating in a Thermal Environment. *Int. J. Struct. Stab. Dyn.* **2022**, *22*, 2250081. [[CrossRef](#)]
57. Asgari, G.R.; Arabali, A.; Babaei, M.; Asemi, K. Dynamic instability of sandwich beams made of isotropic core and functionally graded graphene platelets-reinforced composite face sheets. *Int. J. Struct. Stab. Dyn.* **2022**, *22*, 2250092. [[CrossRef](#)]
58. Javani, M.; Kiani, Y.; Eslami, M. Thermal buckling of FG graphene platelet reinforced composite annular sector plates. *Thin Walled Struct.* **2020**, *148*, 106589. [[CrossRef](#)]
59. Bi, S.; Zhang, E.; Babaei, M.; Tornabene, F.; Dimitri, R. The Influence of GPL Reinforcements on the Post-Buckling Behavior of FG Porous Rings Subjected to an External Pressure. *Mathematics* **2023**, *11*, 2421. [[CrossRef](#)]
60. Rostami, H.; Salami, S.J. Large amplitude free vibration of sandwich beams with flexible core and FG Graphene Platelet Reinforced Composite (FG-GPLRC) face sheets based on extended higher-order sandwich panel theory. *Thin Walled Struct.* **2022**, *180*, 109999. [[CrossRef](#)]
61. Kiani, Y.; Żur, K.K. Free vibrations of graphene platelet reinforced composite skew plates resting on point supports. *Thin Walled Struct.* **2022**, *176*, 109363. [[CrossRef](#)]
62. Kiarasi, F.; Babaei, M.; Sarvi, P.; Asemi, K.; Hosseini, M.; Omid Bidgoli, O. A review on functionally graded porous structures reinforced by graphene platelets. *J. Comput. Appl. Mech.* **2021**, *52*, 731–750.
63. Wu, H.; Zheng, Z.; Guo, J.; Li, L.; Bao, Y.; Yang, J. Axisymmetric thermal postbuckling of functionally graded graphene nanocomposite annular plates with various geometric imperfections. *Thin Walled Struct.* **2023**, *185*, 110594. [[CrossRef](#)]
64. Babaei, M.; Asemi, K.; Kiarasi, F. Static response and free-vibration analysis of a functionally graded annular elliptical sector plate made of saturated porous material based on 3D finite element method. *Mech. Based Des. Struct. Mach.* **2023**, *51*, 1272–1296. [[CrossRef](#)]
65. Van Vinh, P. A new first-order mixed beam element for static bending analysis of functionally graded graphene oxide powder-reinforced composite beams. *Structures* **2022**, *36*, 463–472. [[CrossRef](#)]
66. Arshid, E.; Amir, S.; Loghman, A. Static and dynamic analyses of FG-GNPs reinforced porous nanocomposite annular micro-plates based on MSGT. *Int. J. Mech. Sci.* **2020**, *180*, 105656. [[CrossRef](#)]
67. Babaei, M.; Kiarasi, F.; Asemi, K.; Dimitri, R.; Tornabene, F. Transient Thermal Stresses in FG Porous Rotating Truncated Cones Reinforced by Graphene Platelets. *Appl. Sci.* **2022**, *12*, 3932. [[CrossRef](#)]
68. Lam, K.Y.; Qian, W. Free vibration of symmetric angle-ply thick laminated composite cylindrical shells. *Compos. Part B Eng.* **2000**, *31*, 345–354. [[CrossRef](#)]
69. Mollaei, S.; Babaei, M.; Asemi, K. Torsional buckling of functionally graded graphene reinforced composite laminated cylindrical panel. *Arch. Appl. Mech.* **2023**, *93*, 427–435. [[CrossRef](#)]
70. Nguyen, V.L.; Limkatanyu, S.; Bui, T.Q.; Rungamornrat, J. Free vibration analysis of rotating stiffened functionally graded graphene-platelet-reinforced composite toroidal shell segments with novel four-unknown refined theories. *Int. J. Mech. Mater. Des.* **2023**, *19*, 319–350. [[CrossRef](#)]
71. Nazari, H.; Babaei, M.; Kiarasi, F.; Asemi, K. Geometrically nonlinear dynamic analysis of functionally graded material plate excited by a moving load applying first-order shear deformation theory via generalized differential quadrature method. *SN Appl. Sci.* **2021**, *3*, 1–32. [[CrossRef](#)]
72. Dong, D.T.; Van Dung, D. A third-order shear deformation theory for nonlinear vibration analysis of stiffened functionally graded material sandwich doubly curved shallow shells with four material models. *J. Sandw. Struct. Mater.* **2019**, *21*, 1316–1356. [[CrossRef](#)]
73. Zienkiewicz, O.C.; Taylor, R.L. *The Finite Element Method: Solid Mechanics*; Butterworth-Heinemann: Oxford, UK, 2000.

Disclaimer/Publisher’s Note: The statements, opinions and data contained in all publications are solely those of the individual author(s) and contributor(s) and not of MDPI and/or the editor(s). MDPI and/or the editor(s) disclaim responsibility for any injury to people or property resulting from any ideas, methods, instructions or products referred to in the content.